scSiameseClu: A Siamese Clustering Framework for Interpreting Single-cell RNA Sequencing Data

Ping Xu[1,2] , **Zhiyuan Ning**[1,2] , **Pengjiang Li**[1,2] , **Wenhao Liu**[3] , **Pengyang Wang**[4*] ,
Jiaxu Cui[5] , **Yuanchun Zhou**[1,2] and **Pengfei Wang**[1,2*]

[1]Computer Network Information Center, Chinese Academy of Sciences, Beijing
[2]University of Chinese Academy of Sciences, Beijing
[3]College of Life Science, Northeast Agricultural University, Harbin
[4]SKL-IOTSC and Department of CIS, University of Macau, Macau
[5]Jilin University, Changchun

{xuping, ningzhiyuan, pjli}@cnic.cn, b230901013@neau.edu.cn,
pywang@um.edu.mo, cjx@jlu.edu.cn, {zyc,pfwang}@cnic.cn

Abstract

Single-cell RNA sequencing (scRNA-seq) reveals cell heterogeneity, with cell clustering playing a key role in identifying cell types and marker genes. Recent advances, especially graph neural networks (GNNs)-based methods, have significantly improved clustering performance. However, the analysis of scRNA-seq data remains challenging due to noise, sparsity, and high dimensionality. Compounding these challenges, GNNs often suffer from over-smoothing, limiting their ability to capture complex biological information. In response, we propose **scSiameseClu**, a novel **Siamese Clu**stering framework for interpreting **s**ingle-**c**ell RNA-seq data, comprising of 3 key steps: (1) Dual Augmentation Module, which applies biologically informed perturbations to the gene expression matrix and cell graph relationships to enhance representation robustness; (2) Siamese Fusion Module, which combines cross-correlation refinement and adaptive information fusion to capture complex cellular relationships while mitigating over-smoothing; and (3) Optimal Transport Clustering, which utilizes Sinkhorn distance to efficiently align cluster assignments with predefined proportions while maintaining balance. Comprehensive evaluations on seven real-world datasets demonstrate that scSiameseClu outperforms state-of-the-art methods in single-cell clustering, cell type annotation, and cell type classification, providing a powerful tool for scRNA-seq data interpretation.

1 Introduction

Single-cell RNA sequencing (scRNA-seq) technology represents a significant advancement in bioinformatics, enabling

---

[*]Corresponding authors.

[†]Code and datasets are all available at the link: https://github.com/ XPgogogo/scSiameseClu.
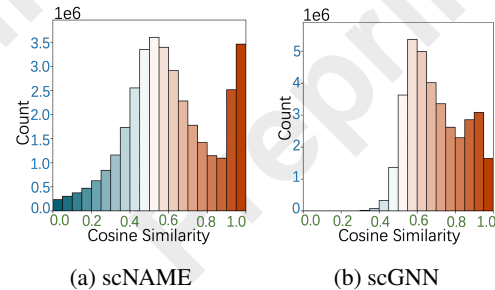

Figure 1: Similarity distributions of cell embeddings learned by scNAME and scGNN on dataset *Human liver cells*.

the capture of comprehensive genetic information from individual cells [Shapiro *et al.*, 2013]. Cell clustering, a key step in single-cell RNA sequencing analysis, groups cells by their gene expression patterns to uncover the complex characteristics of distinct cell populations and provide insights into their biological functions and interactions [Kiselev *et al.*, 2019]. Moreover, clustering gene expression patterns further contributes to various downstream tasks, such as marker gene identification and cell type annotation [Haghverdi *et al.*, 2016]. Cluster analysis of scRNA-seq data has been a vibrant research area over the past decade.

In recent years, advanced computational methods have been increasingly explored to address the challenges of analyzing high-dimensional and sparse scRNA-seq data. Classical clustering methods, such as K-means, are straightforward and computationally efficient but struggle to capture the complex, nonlinear relationships in scRNA-seq data. Meanwhile, recent research has focused on applying deep learning frameworks for learning representations of scRNA-seq data and classifying samples into distinct clusters. A commonly used method is self-supervised learning methods, which uncover effective representations of scRNA-seq data by reconstructing the original input data [Eraslan *et al.*, 2019; Lopez *et al.*, 2018; Tian *et al.*, 2019]. However, these methods primarily focus on extracting features from individual cells, overlooking the

complex relationships between cells that are essential for understanding cellular diversity. Benefiting from the powerful utilization of graph information, graph neural networks (GNNs) have been applied to analyze scRNA-seq data by modeling cells as nodes and their interactions as edges, effectively capturing both gene expressions and cell graphs to comprehensively represent cellular heterogeneity [Wang *et al.*, 2021b; Gan *et al.*, 2022; Zhan *et al.*, 2023].

Though good performance has been achieved, previous GNN-based works still face limitations when tackling the following challenges: **(1) Deficient exploration on intercellular information:** when applying GNN-based models to single-cell data, the graph construction process often overlooks the sparsity and noise inherent in scRNA-seq data, frequently leading to reduced model robustness. Most current methods rely on simple topologies, like cosine similarity, to build cell graphs from gene expression matrices [Gan *et al.*, 2022; Wang *et al.*, 2021c], but do not handle the sparsity and noise inherent in scRNA-seq data. This leads to fragile graph representations, weakening GNNs' ability to capture cellular interactions and limiting clustering performance and insights into cellular dynamics. **(2) Insufficient prevention of representation collapse in cell embeddings:** GNNs-based models for scRNA-seq data frequently encounter representation collapse, where embeddings of biologically distinct cells become overly similar in latent space. This issue arises from the inability of current methods to preserve the diversity of cell representations in sparse and noisy scRNA-seq data. As shown in Fig.1, both the deep learning-based scNAME [Wan *et al.*, 2022] and the GNN-based scGNN [Wang *et al.*, 2021b] exhibit varying degrees of representation collapse. The problem is more pronounced in scGNN, where the cosine similarity between almost all cell embeddings exceeds 0.5, indicating a severe loss of diversity in cell embeddings. Such collapse diminishes the discriminative power of embeddings, blurring cluster boundaries and limiting the ability to distinguish different cell populations, ultimately degrading the effectiveness of GNN models in clustering tasks [Zbontar *et al.*, 2021].

To tackle the aforementioned challenge, we propose **scSiameseClu**, a **Siamese Clu**stering framework for interpreting **s**ingle-**c**ell RNA sequencing data. scSiameseClu is designed to capture and refine complex intercellular information while learning discriminative and robust representations across both gene and cellular features. scSiameseClu leverages three key components: dual augmentation module to enrich data, siamese fusion module to preserve critical information and reduce redundancy, and optimal transport clustering to align cluster distributions. It effectively explores intricate information, mitigates representation collapse, and achieves clearer cell population separation, excelling in scRNA-seq clustering and other biological tasks.

Our framework offers the following contributions:

- We present scSiameseClu, a novel Siamese-based clustering framework tailored for scRNA-seq data that captures intricate information from gene expression and cell graphs to learn discriminative and robust cell embeddings, improving clustering outcomes and downstream tasks.

- We introduce key components: (i) dual augmentation

with distinct noise on gene expression and cell graphs to mitigate dropout effects and improve robustness; (ii) siamese fusion for cross-correlation and adaptive information fusion to enhance robustness; and (iii) optimal transport clustering to align distributions.

- Experimental results on seven datasets demonstrate that scSiameseClu outperforms state-of-the-art (SOTA) methods in clustering and other biological tasks.

2 Related Work

Deep Clustering for scRNA-seq. In scRNA-seq data analysis, early clustering algorithms like Phenograph [Levine *et al.*, 2015], MAGIC [Van Dijk *et al.*, 2018], and Seurat [Wang *et al.*, 2025] utilize k-nearest neighbor (KNN) graphs to model cell relationships, while SIMLR [Wang *et al.*, 2018] and MPSSC [Park and Zhao, 2018] employ multiple kernel functions to derive robust similarity measures from different data representations. These methods, however, often struggle with high-dimensional data and complex nonlinear features, making them susceptible to noise. Deep learning approaches have since become prominent. DCA [Eraslan *et al.*, 2019] employs a Zero-Inflated Negative Binomial (ZINB) autoencoder to model scRNA-seq data distributions, capturing nonlinear gene dependencies. SCVI [Lopez *et al.*, 2018] and SCVIS [Ding *et al.*, 2018], which rely on autoencoders for dimensionality reduction, often face over-regularization due to their Gaussian distribution assumption. Additionally, scDeepCluster [Tian *et al.*, 2019] combines ZINB-based autoencoders with deep embedding clustering to optimize feature learning and clustering. Most approaches ignore inter-gene and inter-cell correlations, focusing solely on individual cell expression profiles.

Graph Clustering for scRNA-seq. Recently, graph-based clustering methods have gained considerable attention for their effectiveness [Tu *et al.*, 2021; Liu *et al.*, 2022; Ning *et al.*, 2025]. Methods like scGAE [Luo *et al.*, 2021] and graph-sc [Ciortan and Defrance, 2022] utilize graph autoencoders to embed scRNA-seq data while preserving topological structures. scGAC [Cheng and Ma, 2022] constructs cell graphs and employs a self-optimization approach for simultaneous representation learning and clustering. Notably, scGNN [Wang *et al.*, 2021b] uses GNNs and multi-modal autoencoders to aggregate cell-cell relationships and model gene expression patterns, while scDSC [Gan *et al.*, 2022] combines a ZINB model-based autoencoder with GNN modules using a mutually supervised strategy. These methods often struggle with representation collapse, severely limiting their ability to accurately model cell relationships.

3 Methodology

This section introduces the proposed scSiameseClu, including the highlighted dual augmentation module, siamese fusion module, optimal transport clustering. More details are provided in the supplementary material, e.g., gene expression autoencoders (GEAs) and cell graph autoencoders (CGAs).

3.1 Problem Formulation

Given a single-cell expression matrix $\mathbf{X} \in \mathbb{R}^{N \times D}$, where $x_{ij} \, (1 \leq i \leq N, 1 \leq j \leq D)$ shows the expression of the j-
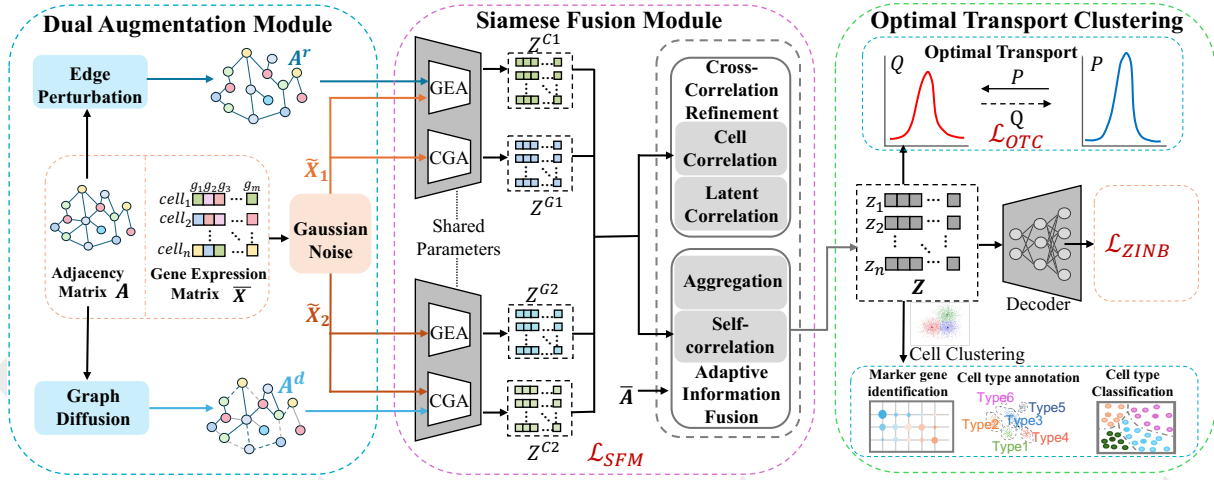
Figure 2: Overview architecture of scSiameseClu. It contains three components: (i) a data-augmented module, (ii) a Siamese fusion module, and (iii) an optimal transport clustering strategy for self-supervision learning.

th gene in the i-th cell. We construct an undirected graph $\mathcal{G}_{\mathcal{C}} = (\mathcal{V}, \mathcal{E})$ using KNN based on the gene expression matrix, where $\mathcal{V} = \{v_1, v_2, \cdots, v_N\}$ is the set of N nodes, $\mathcal{E}$ is the set of edges. Each node corresponds to a single cell, and edges indicate similarity between cells, quantified with the Pearson Correlation Coefficient [Ding *et al.*, 2022; Lu *et al.*, 2022]. The KNN graph is defined with the preprocessed data matrix $\bar{\mathbf{X}}$, as specified in Section 4.1, and adjacency matrix $\mathbf{A} = (a_{ij})_{N \times N}$, where $a_{ij} = 1$ if v_i and v_j are connected, and $a_{ij} = 0$, otherwise. The associated degree matrix is $\mathbf{D} = diag(d_1, d_2, \cdots, d_N) \in \mathbb{R}^{N \times N}$, where $d_i = \sum_{(v_i, v_j) \in \mathcal{E}} a_{ij}$ represents the degree of node v_i. To account for self-loops and normalize the adjacency matrix, we compute $\widetilde{\mathbf{A}} \in \mathbb{R}^{N \times N}$ as $\mathbf{D}^{-1}(\mathbf{A} + \mathbf{I})$, where $\mathbf{I} \in \mathbb{R}^{N \times N}$ is the identity matrix. Our goal is to partition the graph $\mathcal{G}_{\mathcal{C}}$ into $\mathbf{C}$ categories by assigning each node $v_i \in \mathcal{V}$ to one of the $\mathbf{C}$ categories based on $\mathcal{E}$ and gene expression features.

3.2 Framework Overview

We propose **scSiameseClu**, an enhanced graph autoencoder-based siamese clustering framework for interpreting scRNA-seq data. We aim to improve the performance of scRNA-seq clustering and related downstream tasks by learning more accurate and distinctive cell embeddings. As Fig. 2 shows, our framework consists of three components: (i) a dual augmentation module that enhances the gene expression matrix and the cell graph relationships; (ii) a siamese fusion module to map the augmented data into a lower-dimensional latent space, generating cell embeddings; and (iii) an optimal transport clustering strategy for self-supervision learning, which refines the latent representations and generates clustering assignments.

3.3 Dual Augmentation Module

To enhance robustness against noise and generalization across diverse datasets, biologically plausible augmentations are introduced at both gene and cell levels. These augmentations capture the variation in scRNA-seq, helping the model extract biologically meaningful representations.

Gene Expression Augmentation. To enhance robustness at the gene level, biologically plausible augmentations are introduced by adding controlled noise to the gene expression profiles. Specifically, Gaussian noise is applied to simulate natural variability in gene expression. Let $\odot$ denote the Hadamard product [Horn, 1990], and $\mathbf{N} \in \mathbb{R}^{N \times D}$ represent a random noise matrix drawn from a Gaussian distribution $\mathcal{N}(1, 0.1)$. The augmented gene expression matrix $\widetilde{\mathbf{X}}$ is computed as:

$$\widetilde{\mathbf{X}} = \bar{\mathbf{X}} \odot \mathbf{N}, \tag{1}$$

as illustrated in Fig. 2, two augmented gene expression matrices, $\widetilde{\mathbf{X}}_1$ and $\widetilde{\mathbf{X}}_2$, were generated using Gaussian distributions with distinct parameters.

Cell Graph Augmentation. Cell graph augmentation aims to improve model robustness and enhance representation learning by introducing perturbations to the cell graph, specifically through edge perturbation and graph diffusion [Wang *et al.*, 2024]. These two strategies provide distinct, yet complementary, perspectives on the cell graph, enabling the model to capture diverse interactions between cells.

(i) *Edge perturbation.* We employ an edge removal strategy to refine the cell graph while preserving the most meaningful and biologically relevant relationships. Removing weaker edges reduces graph noise and improves model robustness. In contrast, edge addition is avoided to prevent spurious connections that may distort the graph and compromise its biological validity. Specifically, a mask matrix $\mathbf{M} \in \mathbb{R}^{N \times N}$ is constructed based on the pairwise cosine similarity matrix computed in the latent space. The 10% of edges with the lowest similarity values are identified and removed using this mask. Finally, the adjacency matrix $\mathbf{A}^r \in \mathbb{R}^{N \times N}$ is normalized for proper scaling, calculated as:

$$\mathbf{A}^r = \mathbf{D}^{-\frac{1}{2}}((\mathbf{A} \odot \mathbf{M}) + \mathbf{I})\mathbf{D}^{-\frac{1}{2}}. \tag{2}$$

(ii) *Graph diffusion.* We use a graph diffusion strategy to refine the cell graph by enhancing meaningful relationships between cells [Hassani and Khasahmadi, 2020]. Specifically,

the normalized adjacency matrix is transformed into a diffusion adjacency matrix using the Personalized PageRank (PPR) algorithm [Page *et al.*, 1998]. The teleport probability controls information propagation across the graph, helping to emphasize biologically meaningful relationships. The diffusion adjacency matrix $\mathbf{A}^d$ would be computed as:

$$\mathbf{A}^d = \alpha \left(\mathbf{I} - (1-\alpha) \left(\mathbf{D}^{-\frac{1}{2}}(\mathbf{A}+\mathbf{I})\mathbf{D}^{-\frac{1}{2}} \right) \right)^{-1}, \quad (3)$$

Thus, we define two distinct adjacency matrices, $\mathbf{A}^r$ and $\mathbf{A}^d$, from edge perturbation and graph diffusion, respectively.

3.4 Siamese Fusion Module

We propose the Siamese Fusion Module (**SFM**), a novel framework that integrates cross-correlation refinement and adaptive information fusion to learn discriminative and robust sample representations and avoid the over-smoothing issue of GNN-based methods [Ning *et al.*, 2022]. By minimizing the deviation of cross-correlation matrices from the ideal identity matrix across cells and genes and adaptive information fusion, SFM effectively reduces redundancy while preserving critical information [Zbontar *et al.*, 2021; Tu *et al.*, 2021; Liu *et al.*, 2022]. This enhances the cell representations and avoids representation collapse, enabling more accurate cell population separation and improving clustering performance.
Cross-Correlation Refinement. The cross-correlation refinement process is designed to effectively encode and integrate the augmented data from genes and cells, ensuring the information from different augmentations is unified. We construct two gene expression autoencoders (GEAs) to process the augmented gene expression matrices $\widetilde{\mathbf{X}}_1$ and $\widetilde{\mathbf{X}}_2$, generating gene expression embeddings $\mathbf{Z}^{G1} \in \mathbb{R}^{N \times d}$ and $\mathbf{Z}^{G2} \in \mathbb{R}^{N \times d}$, where d represents the latent embedding dimensionality. Similarly, we construct two cell graph autoencoders (CGAs) to process the augmented cell graph matrices $\widetilde{\mathbf{X}}_1, \mathbf{A}^r$ and $\widetilde{\mathbf{X}}_2, \mathbf{A}^d$, producing cell graph embeddings $\mathbf{Z}^{C1} \in \mathbb{R}^{N \times d}$ and $\mathbf{Z}^{C2} \in \mathbb{R}^{N \times d}$.
Cell Correlation Refinement. Cell correlation refinement (CCR) optimizes cell relationships across different augmented views by aligning corresponding embeddings and reducing redundant correlations. We can calculate the refined cell correlation matrix by $\mathbf{R}_{ij}^{C1} = \frac{(\mathbf{z}_i^{G1})(\mathbf{z}_j^{G2})^{\mathrm{T}}}{\|\mathbf{z}_i^{G1}\|\|\mathbf{z}_j^{G2}\|}, \mathbf{R}_{ij}^{C2} = \frac{(\mathbf{z}_i^{C1})(\mathbf{z}_j^{C2})^{\mathrm{T}}}{\|\mathbf{z}_i^{C1}\|\|\mathbf{z}_j^{C2}\|}, \forall i,j \in [1,N].$

To ensure the cell correlation matrix $\mathbf{R}^{C1}, \mathbf{R}^{C2}$ aligns with an identity matrix $\mathbf{I}^C \in \mathbb{R}^{N \times N}$, we minimize loss:

$$\mathcal{L}_{Cor1} = \frac{1}{N^2} \sum \left(\mathbf{R}^{C1} - \mathbf{I}^C \right)^2 + \frac{1}{N^2} \sum \left(\mathbf{R}^{C2} - \mathbf{I}^C \right)^2 \quad (4)$$

By ensuring the diagonal elements of $\mathbf{R}^{C1}, \mathbf{R}^{C2}$ are equal to 1 and the off-diagonal elements are equal to 0, we can guarantee the alignment of embeddings for each view and minimize the consistency of embeddings for different cells across different views. This helps scSiameseClu reduce redundant information and learn more discriminative representations.

Latent Correlation Refinement. Similarly, latent correlation refinement (LCR) optimizes relationships between latent embeddings across different augmented views by aligning corresponding embeddings. First, we project gene expression embeddings $\mathbf{Z}^{G1}$ and $\mathbf{Z}^{G2}$ into $\widetilde{\mathbf{Z}}^{G1}$ and $\widetilde{\mathbf{Z}}^{G2} \in \mathbb{R}^{d \times K}$ with using a readout function $\mathcal{R}(\cdot) : \mathbb{R}^{d \times N} \to \mathbb{R}^{d \times K}$, formulated as $\widetilde{\mathbf{Z}}^{G1} = \mathcal{R}\left((\mathbf{Z}^{G1})^{\mathrm{T}}\right), \widetilde{\mathbf{Z}}^{G1} = \mathcal{R}\left((\mathbf{Z}^{G2})^{\mathrm{T}}\right)$. Likewise, we can project cell graph embeddings $\mathbf{Z}^{C1}$ and $\mathbf{Z}^{C2}$ into $\widetilde{\mathbf{Z}}^{C1} = \mathcal{R}\left((\mathbf{Z}^{C1})^{\mathrm{T}}\right)$ and $\widetilde{\mathbf{Z}}^{C2} = \mathcal{R}\left((\mathbf{Z}^{C2})^{\mathrm{T}}\right)$.

Then we can calculate the refine latent correlation matrix by $\mathbf{R}_{ij}^{L1} = \frac{(\widetilde{\mathbf{z}}_i^{G1})(\widetilde{\mathbf{z}}_j^{G2})^{\mathrm{T}}}{\|\widetilde{\mathbf{z}}_i^{G1}\|\|\widetilde{\mathbf{z}}_j^{G2}\|}, \mathbf{R}_{ij}^{L2} = \frac{(\widetilde{\mathbf{z}}_i^{C1})(\widetilde{\mathbf{z}}_j^{C2})^{\mathrm{T}}}{\|\widetilde{\mathbf{z}}_i^{C1}\|\|\widetilde{\mathbf{z}}_j^{C2}\|}, \forall i,j \in [1,d]$, which denotes the correlation between the embeddings learned from enhanced gene expression matrix.

To ensure the latent correlation matrix $\mathbf{R}^{L1}, \mathbf{R}^{L2}$ aligns with an identity matrix $\mathbf{I}^L \in \mathbb{R}^{d \times d}$, we minimize the loss:

$$\mathcal{L}_{Cor2} = \frac{1}{d^2} \sum \left(\mathbf{R}^{L1} - \mathbf{I}^L \right)^2 + \frac{1}{d^2} \sum \left(\mathbf{R}^{L2} - \mathbf{I}^L \right)^2 \quad (5)$$

Adaptive Information Fusion. To enhance clustering performance, we propose an adaptive information fusion mechanism that integrates cell relationships through embedding aggregation, self-correlation learning, and dynamic recombination. We first aggregate the embeddings achieved with GEA and CGA with a linear combination operation:

$$\mathbf{Z}^A = \left(\mathbf{Z}^{G1} + \mathbf{Z}^{G2} + \mathbf{Z}^{C1} + \mathbf{Z}^{C2} \right)/4, \quad (6)$$

Then, we apply a graph convolution-like operation (i.e., message passing) to process the combined information, enhancing the initial fused embedding $\mathbf{Z}^A \in \mathbb{R}^{N \times d}$. Specifically, we enhance $\mathbf{Z}^A$ by propagating cell graph $\widetilde{\mathbf{A}}$, i.e., $\mathbf{Z}^E = \widetilde{\mathbf{A}}\mathbf{Z}^A$. To capture the relationships among cell graphs in the enhanced embedding space, we compute a normalized self-correlation matrix $\mathbf{R}^{\mathbf{S}} \in \mathbb{R}^{N \times N}$. Each element of $\mathbf{R}^{\mathbf{S}}$ is defined as $\mathbf{R}^{\mathbf{S}}_{ij} = \frac{exp\left(\left(\mathbf{Z}^E(\mathbf{Z}^E)^{\mathrm{T}} \right)_{ij} \right)}{\sum_{k=1}^{N} exp\left((\mathbf{Z}^E(\mathbf{Z}^E)^{\mathrm{T}})_{ik} \right)}$. The self-correlation matrix $\mathbf{R}^{\mathbf{S}}$ encodes the relative similarity between cells, providing a mechanism to model relationships in the embedding space. Thus, we can recombine the embedding matrix $\mathbf{Z}^E$ to dynamically adjust the embedding representations. Specifically, the recombined embedding matrix $\mathbf{Z}^R$ is computed as $\mathbf{Z}^R = \mathbf{R}^{\mathbf{S}}\mathbf{Z}^E$. Each cell integrates information from others through learned relationships, enhancing embeddings for clustering.

To preserve the initial fused embedding information while incorporating the recombined embeddings, we adopt a skip connection to fuse $\mathbf{Z}^E$ and $\mathbf{Z}^R$. The final clustering-oriented latent embeddings $\mathbf{Z} \in \mathbb{R}^{N \times d}$ are computed as:

$$\mathbf{Z} = \mathbf{Z}^E + \beta\mathbf{Z}^R, \quad (7)$$

where β is a learnable scale parameter, initialized to 0 and updated during training. This fusion mechanism effectively filters out redundant information and preserves discriminative features in the latent space, enabling the network to learn robust and meaningful representations that enhance clustering performance while avoiding representation collapse.
Propagated Regularization. The reconstruction loss, $\mathcal{L}_{REC}$ minimizes the joint mean square error (MSE) of reconstruction

loss of gene expression and cell graph matrix. To further enhance representation quality, we introduce a propagation regularization. Drawing inspiration from [Liu *et al.*, 2022], formulated as follows:

$$\mathcal{L}_R = JSD(\mathbf{Z}, \widetilde{\mathbf{A}}\mathbf{Z}), \qquad (8)$$

where $JSD(\cdot)$ refers the Jensen-Shannon divergence [Fuglede and Topsoe, 2004]. Utilizing Eq. 8, the network can capture long-range dependencies even with a shallow network architecture, thereby reducing over-smoothing as the propagated information deepens within the framework. Finally, the overall objective of the SFM module can be computed by:

$$\mathcal{L}_{SFM} = \mathcal{L}_{Cor1} + \mathcal{L}_{Cor2} + \mathcal{L}_{REC} + \gamma\mathcal{L}_R, \qquad (9)$$

where γ is a trade-off parameter balancing the contribution of the propagation regularization.

3.5 Optimal Transport Clustering

We utilize a self-supervised method to perform unsupervised clustering of scRNA-seq data [Xie *et al.*, 2016], which learn directly from the data without requiring labeled inputs. Specifically, we employ Student's t-distribution [Van der Maaten and Hinton, 2008] as a kernel function to measure the similarity q_{ij} between each cell embedding h_i and the cluster center c_j. By assigning higher weights to closer points, this method effectively captures the non-linear relationships in scRNA-seq data. The assignment distribution is represented as a matrix $Q = [q_{ij}]$, where each element indicates the probability or similarity between sample i and cluster center j. To further refine clustering, we compute a target distribution matrix $P = [p_{ij}]$, which sharpens the soft assignments in Q by emphasizing high-confidence samples. This sharpening process improves cluster separation and ensures well-defined clusters. The clustering process is optimized by minimizing the divergence between Q and P, iteratively refining results to group similar cells and separate dissimilar ones. In the target distribution P, each assignment in Q is squared and normalized to enhance assignment confidence [Bo *et al.*, 2020].

To avoid degenerate solutions that would allocate all data points to a single label, we establish constraints that synchronize the label distribution with the mixing proportions. This ensures that each cell contributes equally to the loss calculation, improving clustering accuracy and preserving a balanced effect during learning process. We construct the target probability matrix P using the following optimal transport strategy to ensure this alignment and enhance the robustness of our clustering outcomes:

$$\min_P - P * (\log Q)$$
$$\text{s.t.} P \in \mathbb{R}_+^{N \times C}, P\,\mathbf{1}_C = \mathbf{1}_N \text{ and } P^T\mathbf{1}_N = N\boldsymbol{\pi}. \qquad (10)$$

In this context, we regard the target distribution P as the transport plan matrix derived from optimal transport theory, while $-\log Q$ serves as the cost matrix. We impose the constraint $P^T\mathbf{1}_N = N\boldsymbol{\pi}$, where π indicates the proportion of cells assigned to each cluster, estimated from intermediate clustering results. Thus, we can ensure that the resulting cluster distribution aligns with the defined mixing proportions. Given the substantial computational expense associated with direct optimization techniques, we utilize the Sinkhorn distance [Sinkhorn,

1967] to facilitate quicker optimization through an entropic constraint. The optimization problem, which includes a Lagrange multiplier for the entropy constraint is formulated as:

$$\min_P - P * (\log Q) - \frac{1}{\lambda}\mathrm{H}(P)$$
$$\text{s.t.} P \in \mathbb{R}_+^{N \times C}, P\,\mathbf{1}_C = \mathbf{1}_N \text{ and } P^T\mathbf{1}_N = N\boldsymbol{\pi}, \qquad (11)$$

where $\boldsymbol{H}$ is the entropy function measuring uncertainty in the distribution, and λ is the smoothness parameter that maintains cluster balance. The transport plan P is guaranteed to exist and be unique, with the solution efficiently obtained through Sinkhorn's method [Sinkhorn, 1967] as follows:

$$\hat{P}^{(t)} = \mathrm{diag}\left(\boldsymbol{u}^{(t)}\right) Q^\lambda \mathrm{diag}\left(\boldsymbol{v}^{(t)}\right) \qquad (12)$$

at each iteration t, $\boldsymbol{u}^{(t)}$ is updated as $\mathbf{1}_N/(Q^\lambda\boldsymbol{v}^{(t-1)})$ and $\boldsymbol{v}$ is calculated as $N_\pi/(Q^\lambda\boldsymbol{u}^{(t)})$. We begin with the initial value set as $\boldsymbol{v}^{(0)} = \mathbf{1}_N$. Upon convergence, the optimal transport plan matrix $\hat{P}$ is obtained.

During training, $\hat{P}$ is fixed and Q is aligned with $\hat{P}$. This alignment is crucial for evaluating model performance, allowing us to define the clustering loss function as follows:

$$\mathcal{L}_{OTC} = \mathrm{KL}(\hat{P}\|Q) = \sum_i \sum_j \hat{p}_{ij} \log \frac{\hat{p}_{ij}}{q_{ij}} \qquad (13)$$

3.6 Joint Optimization

The Zero-Inflated Negative Binomial (ZINB) loss $\mathcal{L}_{ZINB}$ is commonly used to handle the sparsity and overdispersion of scRNA-seq data by modeling excess zeros and variability, ensuring accurate data reconstruction [Eraslan *et al.*, 2019]. Thus, in the proposed method, the overall optimization objective consists of three parts: the SFM loss, the OTC loss, and the ZINB loss, which are formulated as:

$$\mathcal{L} = \mathcal{L}_{SFM} + \rho\mathcal{L}_{ZINB} + \sigma\mathcal{L}_{OTC}, \qquad (14)$$

where the hyperparameters ρ and σ balance the components, facilitating effective embedding learning and clustering.

4 Experiments

In this section, we first validate our method through extensive experiments, demonstrating its superior performance in scRNA-seq clustering. We then show that the embeddings generated by our method effectively mitigate the embedding collapse issue in graph-based models. We also evaluate its utility in downstream tasks, like cell type annotation.

4.1 Experimental Setup

Dataset Preprocessing. We evaluated scSiameseClu on seven real scRNA-seq datasets. First, genes expressed in fewer than three cells were filtered out, followed by normalization, log-transformed (logTPM), and selection of highly variable genes based on predefined mean and dispersion thresholds. Finally, the preprocessed data were used as input.

Baseline Methods. To verify the superior performance of the proposed approach, we compare it against nine competing

Dataset	Metric	pcaReduce	SUSSC	DEC	scDeepCluster	scDCC	scNAME	scDSC	scGNN	scCDCG	OURS
Shekhar mouse retina cells	ACC	21.27 ± 0.14	25.04 ± 0.73	24.55 ± 2.29	47.26 ± 3.34	74.14 ± 2.31	<u>79.84</u> ± 2.77	67.54 ± 4.08	78.56 ± 3.95	76.04 ± 1.85	**89.16** ± 3.52
	NMI	25.54 ± 0.05	43.35 ± 0.36	40.32 ± 3.50	80.45 ± 1.28	<u>81.20</u> ± 0.68	75.19 ± 11.89	62.46 ± 14.53	79.89 ± 5.28	76.71 ± 1.47	**82.72** ± 1.22
	ARI	10.01 ± 0.03	19.69 ± 0.52	17.96 ± 3.59	52.66 ± 5.77	62.44 ± 4.50	<u>81.66</u> ± 7.05	54.53 ± 8.34	77.58 ± 9.59	60.65 ± 6.47	**88.93** ± 2.15
Macosko mouse retina cells	ACC	16.40 ± 0.33	30.34 ± 0.40	33.32 ± 2.97	54.45 ± 3.03	63.31 ± 11.09	<u>78.97</u> ± 7.76	72.16 ± 0.77	62.80 ± 2.26	69.78 ± 0.70	**87.13** ± 2.15
	NMI	23.35 ± 0.19	50.72 ± 0.13	52.20 ± 2.14	76.83 ± 2.09	79.13 ± 0.94	<u>82.64</u> ± 1.44	67.04 ± 0.49	68.25 ± 3.36	68.71 ± 2.52	**86.62** ± 2.31
	ARI	11.44 ± 0.79	18.89 ± 0.53	27.55 ± 6.65	40.90 ± 1.44	52.38 ± 2.78	<u>84.72</u> ± 0.17	61.55 ± 0.82	74.01 ± 2.25	58.99 ± 2.69	**90.92** ± 3.74
QS mouse lung cells	ACC	33.70 ± 0.21	40.82 ± 0.10	38.07 ± 1.40	47.16 ± 3.35	48.29 ± 5.51	69.84 ± 2.77	67.54 ± 4.08	69.46 ± 1.88	<u>70.58</u> ± 0.87	**87.16** ± 1.52
	NMI	16.10 ± 0.54	43.08 ± 0.01	37.27 ± 3.76	70.18 ± 2.24	50.40 ± 7.24	71.41 ± 5.40	69.48 ± 7.11	64.20 ± 2.10	<u>70.13</u> ± 1.92	**86.07** ± 1.04
	ARI	11.68 ± 0.25	28.07 ± 0.04	23.08 ± 3.75	41.37 ± 4.07	42.76 ± 10.05	45.50 ± 3.20	76.76 ± 7.24	75.90 ± 0.97	<u>80.67</u> ± 0.78	**84.49** ± 3.44
CITE-CMBC	ACC	28.15 ± 0.07	47.19 ± 0.02	41.88 ± 5.35	67.59 ± 4.40	69.04 ± 3.46	60.22 ± 5.87	68.79 ± 0.87	66.71 ± 1.65	<u>71.75</u> ± 1.8	**74.70** ± 0.51
	NMI	28.28 ± 0.19	60.14 ± 0.04	46.87 ± 9.23	73.16 ± 1.29	72.83 ± 1.31	48.98 ± 7.06	64.21 ± 3.25	61.70 ± 3.21	<u>68.57</u> ± 1.7	**68.71** ± 0.75
	ARI	5.09 ± 0.04	32.84 ± 4.51	23.55 ± 10.25	51.21 ± 3.40	52.42 ± 2.60	66.06 ± 3.37	52.51 ± 2.15	66.25 ± 1.75	<u>61.06</u> ± 1.4	**67.56** ± 1.17
Human liver cells	ACC	35.04 ± 0.14	47.96 ± 0.06	46.32 ± 6.76	61.32 ± 8.61	72.90 ± 4.02	74.55 ± 5.30	70.90 ± 2.23	72.33 ± 3.4	<u>75.34</u> ± 1.7	**88.33** ± 1.74
	NMI	32.43 ± 0.33	67.17 ± 0.00	52.24 ± 3.44	78.09 ± 2.50	78.81 ± 1.50	77.42 ± 12.00	71.63 ± 2.75	73.56 ± 2.7	<u>79.34</u> ± 2.6	**88.82** ± 1.24
	ARI	10.24 ± 1.42	35.27 ± 0.00	31.04 ± 10.90	58.28 ± 10.61	70.47 ± 1.93	79.91 ± 2.93	75.34 ± 3.56	76.01 ± 2.6	<u>81.26</u> ± 2.7	**91.90** ± 0.48
Human kidney cells	ACC	41.38 ± 0.24	44.18 ± 0.22	38.91 ± 2.71	59.81 ± 4.69	67.89 ± 6.22	73.71 ± 3.90	75.32 ± 2.81	77.73 ± 1.41	<u>79.55</u> ± 0.29	**86.08** ± 0.89
	NMI	24.31 ± 0.13	37.35 ± 0.02	28.78 ± 5.10	63.67 ± 3.70	66.53 ± 4.91	61.39 ± 4.70	69.41 ± 2.12	<u>73.79</u> ± 1.07	67.98 ± 2.62	**80.86** ± 0.96
	ARI	24.56 ± 0.29	30.78 ± 0.02	19.97 ± 5.06	47.53 ± 5.44	50.37 ± 7.22	68.39 ± 2.41	67.74 ± 4.52	<u>72.29</u> ± 1.59	64.91 ± 0.88	**74.23** ± 2.07
Human pancreas cells	ACC	51.17 ± 0.66	76.29 ± 0.02	72.22 ± 5.51	74.70 ± 2.69	86.65 ± 5.76	89.63 ± 5.83	79.42 ± 1.34	79.32 ± 3.96	<u>92.65</u> ± 1.9	**94.95** ± 0.15
	NMI	57.71 ± 0.67	82.31 ± 0.13	76.29 ± 2.73	79.32 ± 0.32	83.81 ± 2.94	86.70 ± 7.79	75.89 ± 0.61	78.76 ± 5.60	<u>85.81</u> ± 1.0	**86.19** ± 0.34
	ARI	37.00 ± 0.45	64.24 ± 0.01	61.76 ± 5.55	64.59 ± 2.49	79.83 ± 10.79	84.93 ± 3.13	75.42 ± 1.22	78.81 ± 3.17	<u>91.37</u> ± 1.21	**91.59** ± 0.35

Table 1: Clustering performance across seven datasets (mean ± standard deviation), with best results in **bold** and runner-up results in <u>underline</u>.

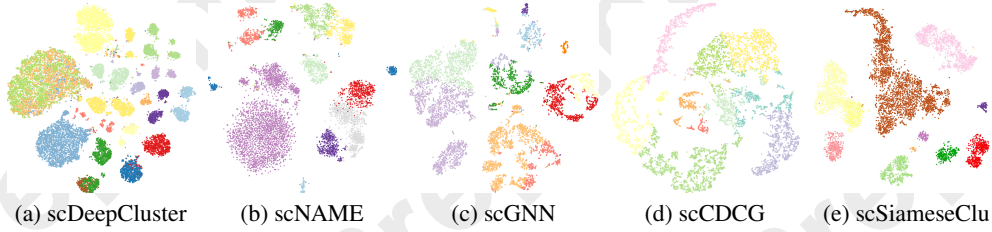(a) scDeepCluster (b) scNAME (c) scGNN (d) scCDCG (e) scSiameseClu

Figure 3: Visualization of scSiameseClu and four typical baselines on *human liver cells* in 2D t-SNE projection. Each point represents a cell, while each color represents a predicted cell type.

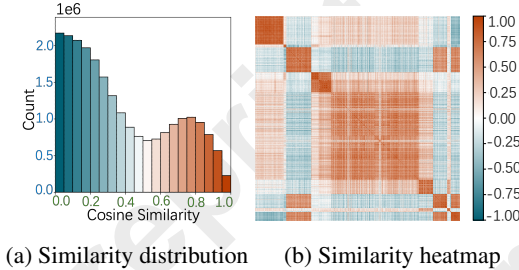(a) Similarity distribution (b) Similarity heatmap

Figure 4: Distribution plot and heat map of cell similarities in latent space learned by scSiameseClu on the *Human liver cells* dataset.

SOTA clustering methods. Among them, pcaReduce [Žurauskienė and Yau, 2016] and SUSSC [Wang et al., 2021a] represent early traditional clustering techniques. Additionally, we consider four deep neural network-based clustering methods, DEC [Xie et al., 2016], scDeepCluster [Tian et al., 2019], scDCC [Tian et al., 2021], and scNAME [Wan et al., 2022], which train an autoencoder to obtain representations followed by clustering. scDSC [Gan et al., 2022], scGNN [Wang et al., 2021b], and scCDCG [Xu et al., 2024] are representative GNN-based clustering methods that incorporate both node attributes and structural information for latent representation.

Implementation Details. We implemented scSiameseClu in Python 3.7 using PyTorch, with DCRN [Liu et al., 2022] as the backbone. Each experiment was repeated 10 times,

reporting the mean and variance. Detailed parameter settings are provided in the supplementary material.

Evaluation Metrics. To illustrate the effectiveness of our approach, we evaluate clustering performance through three widely recognized metrics: Accuracy (ACC), Normalized Mutual Information (NMI) [Strehl and Ghosh, 2002], and Adjusted Rand Index (ARI) [Vinh et al., 2009].

4.2 Overall Performance

Quantitative Analysis. Tab. 1 compares the clustering performance of our method with nine competitive baselines across seven benchmark datasets. Based on the results, we can observe that: 1) scSiameseClu significantly outperforms traditional single-cell clustering methods, demonstrating its superior ability to handle scRNA-seq data. 2) Compared to deep learning-based methods, which rely solely on node information for clustering, scSiameseClu achieves consistently better results, highlighting its ability to leverage both gene and cell information effectively. 3) While GNN-based methods incorporate cell graph information, they suffer from redundant embeddings and representation collapse. In contrast, scSiameseClu learns more discriminative representations of scRNA-seq data, thereby enhancing clustering performance. Overall, scSiameseClu outperforms the competing methods on three metrics across all datasets. On average, scSiameseClu achieves a significant average improvement of 8.41% in ACC, 5.89% in NMI, 4.34% in ARI than the second-best method.

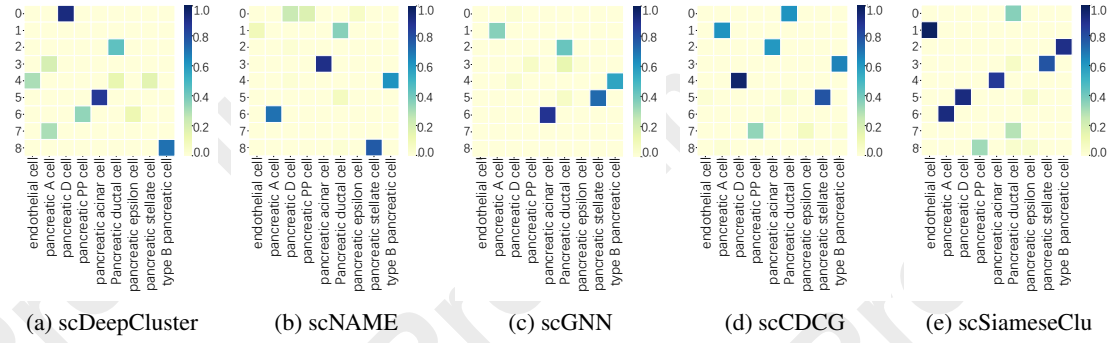**Qualitative Analysis.** To evaluate clustering performance,

(a) scDeepCluster   (b) scNAME   (c) scGNN   (d) scCDCG   (e) scSiameseClu

Figure 5: Cell type annotation: overlap of top 50 DEGs in clusters versus gold standard cell types (similarity = overlapping DEGs/50).

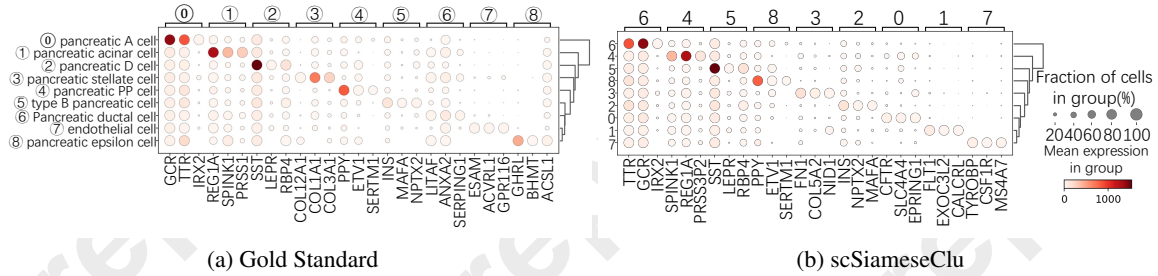(a) Gold Standard   (b) scSiameseClu

Figure 6: Top 3 DEGs per cell type annotated by scSiameseClu and gold standard.

we used t-SNE to project the learned embeddings from different methods into a two-dimensional space on the *Human liver cells* dataset. As Fig. 3 shows, scSiameseClu produces well-separated clusters with clear boundaries, effectively distinguishing different cell types regardless of cluster size. In contrast, methods like scDeepCluster show dispersed clusters, failing to group similar cell types. We further analyze the embeddings from scSiameseClu with the cosine similarity matrices. As shown in Fig. 4, the bimodal distribution of cosine similarities (approaching a multivariate Gaussian) and the distinct heatmap patterns preserve meaningful cluster structures in the latent space. scSiameseClu mitigates representation collapse and effectively captures latent cluster structures, unlike other deep learning and GNN-based methods (Fig1).

4.3 Biological Analysis

Cell Type Annotation. To demonstrate that our clustering method enables more effective downstream analysis, we first identified differentially expressed genes (DEGs) and marker genes for each cluster using the "FindAllMarkers" function in Seurat [Butler *et al.*, 2018]. Then, we compared the top 50 marker genes identified by scSiameseClu and other methods to the gold standard on the *human pancreas cells* dataset, and our method accurately annotated clusters with cell types, achieving over 90% similarity in marker genes for most clusters. As Fig. 5 shows, cluster 1 was identified as endothelial cell type, and cluster 2 as type B pancreatic cells, etc. Additionally, Fig. 6 shows scSiameseClu identifies marker genes for each cluster, e.g., cluster 6 is characterized as pancreatic A cell type with marker genes TTR, GCG, and IRX2. Our method

Metric	pcaReduce	scDCC	scDSC	scCDCG	scGNN	scSiameseClu
Accuracy	83.17	86.34	91.71	98.05	99.02	**99.51**
Precision	57.40	66.69	89.30	92.70	88.50	**99.69**
Recall	49.34	67.65	79.41	93.45	98.98	**99.09**
F1	48.17	65.82	78.84	93.06	99.23	**99.36**

Table 2: Classification performance comparison.

effectively matched clusters with known cell types, providing reliable support for mechanistic studies.

Cell Type Classification. To evaluate the discriminative power and generalization ability of the learned representations, we conducted classification experiments. Tab. 2 shows that scSiameseClu outperforms the baseline models on *human pancreatic cells* dataset across four metrics, including accuracy and F1-score. This demonstrates scSiameseClu's superior performance in identifying cellular heterogeneity and the robustness and effectiveness in cell type classification.

5 Conclusion

scSiameseClu integrates dual augmentation module, siamese fusion module, and optimal transport clustering to enhance representation learning while preserving biological relevance. Experimental results on seven datasets demonstrate that scSiameseClu not only outperforms nine baselines on scRNA-seq clustering but also alleviates the representation collapse issue common in GNN-based approaches. In addition, we conduct biological analyses, including cell type annotation and classification, underscoring the scSiameseClu's potential as a powerful tool for advancing single-cell transcriptomics.

References

[Bo *et al.*, 2020] Deyu Bo, Xiao Wang, Chuan Shi, Meiqi Zhu, Emiao Lu, and Peng Cui. Structural deep clustering network. In *Proceedings of the web conference 2020*, pages 1400–1410, 2020.

[Butler *et al.*, 2018] Andrew Butler, Paul Hoffman, Peter Smibert, Efthymia Papalexi, and Rahul Satija. Integrating single-cell transcriptomic data across different conditions, technologies, and species. *Nature biotechnology*, 36(5):411–420, 2018.

[Cheng and Ma, 2022] Yi Cheng and Xiuli Ma. scgac: a graph attentional architecture for clustering single-cell rna-seq data. *Bioinformatics*, 38(8):2187–2193, 2022.

[Ciortan and Defrance, 2022] Madalina Ciortan and Matthieu Defrance. Gnn-based embedding for clustering scrna-seq data. *Bioinformatics*, 38(4):1037–1044, 2022.

[Ding *et al.*, 2018] Jiarui Ding, Anne Condon, and Sohrab P Shah. Interpretable dimensionality reduction of single cell transcriptome data with deep generative models. *Nature communications*, 9(1):2002, 2018.

[Ding *et al.*, 2022] Kaize Ding, Zhe Xu, Hanghang Tong, and Huan Liu. Data augmentation for deep graph learning: A survey. *ACM SIGKDD Explorations Newsletter*, 24(2):61–77, 2022.

[Eraslan *et al.*, 2019] Gökcen Eraslan, Lukas M Simon, Maria Mircea, Nikola S Mueller, and Fabian J Theis. Single-cell rna-seq denoising using a deep count autoencoder. *Nature communications*, 10(1):390, 2019.

[Fuglede and Topsoe, 2004] Bent Fuglede and Flemming Topsoe. Jensen-shannon divergence and hilbert space embedding. In *International symposium onInformation theory, 2004. ISIT 2004. Proceedings.*, page 31. IEEE, 2004.

[Gan *et al.*, 2022] Yanglan Gan, Xingyu Huang, Guobing Zou, Shuigeng Zhou, and Jihong Guan. Deep structural clustering for single-cell rna-seq data jointly through autoencoder and graph neural network. *Briefings in Bioinformatics*, 23(2):bbac018, 2022.

[Haghverdi *et al.*, 2016] Laleh Haghverdi, Maren Büttner, F Alexander Wolf, Florian Buettner, and Fabian J Theis. Diffusion pseudotime robustly reconstructs lineage branching. *Nature methods*, 13(10):845–848, 2016.

[Hassani and Khasahmadi, 2020] Kaveh Hassani and Amir Hosein Khasahmadi. Contrastive multi-view representation learning on graphs. In *International conference on machine learning*, pages 4116–4126. PMLR, 2020.

[Horn, 1990] Roger A Horn. The hadamard product. In *Proc. Symp. Appl. Math*, volume 40, pages 87–169, 1990.

[Kiselev *et al.*, 2019] Vladimir Yu Kiselev, Tallulah S Andrews, and Martin Hemberg. Challenges in unsupervised clustering of single-cell rna-seq data. *Nature Reviews Genetics*, 20(5):273–282, 2019.

[Levine *et al.*, 2015] Jacob H Levine, Erin F Simonds, Sean C Bendall, Kara L Davis, D Amir El-ad, Michelle D Tadmor, Oren Litvin, Harris G Fienberg, Astraea Jager, Eli R Zunder, et al. Data-driven phenotypic dissection of aml reveals progenitor-like cells that correlate with prognosis. *Cell*, 162(1):184–197, 2015.

[Liu *et al.*, 2022] Yue Liu, Wenxuan Tu, Sihang Zhou, Xinwang Liu, Linxuan Song, Xihong Yang, and En Zhu. Deep graph clustering via dual correlation reduction. In *Proceedings of the AAAI conference on artificial intelligence*, volume 36, pages 7603–7611, 2022.

[Lopez *et al.*, 2018] Romain Lopez, Jeffrey Regier, Michael B Cole, Michael I Jordan, and Nir Yosef. Deep generative modeling for single-cell transcriptomics. *Nature methods*, 15(12):1053–1058, 2018.

[Lu *et al.*, 2022] Jianchao Lu, Yuzhe Tian, Shuang Wang, Michael Sheng, and Xi Zheng. Pearnet: A pearson correlation-based graph attention network for sleep stage recognition. In *2022 IEEE 9th International Conference on Data Science and Advanced Analytics (DSAA)*, pages 1–8. IEEE, 2022.

[Luo *et al.*, 2021] Zixiang Luo, Chenyu Xu, Zhen Zhang, and Wenfei Jin. A topology-preserving dimensionality reduction method for single-cell rna-seq data using graph autoencoder. *Scientific reports*, 11(1):20028, 2021.

[Ning *et al.*, 2022] Zhiyuan Ning, Pengfei Wang, Pengyang Wang, Ziyue Qiao, Wei Fan, Denghui Zhang, Yi Du, and Yuanchun Zhou. Graph soft-contrastive learning via neighborhood ranking. *arXiv preprint arXiv:2209.13964*, 2022.

[Ning *et al.*, 2025] Zhiyuan Ning, Zaitian Wang, Ran Zhang, Ping Xu, Kunpeng Liu, Pengyang Wang, Wei Ju, Pengfei Wang, Yuanchun Zhou, Erik Cambria, et al. Deep cut-informed graph embedding and clustering. *arXiv preprint arXiv:2503.06635*, 2025.

[Page *et al.*, 1998] Lawrence Page, Sergey Brin, Rajeev Motwani, and Terry Winograd. The pagerank citation ranking: Bring order to the web. Technical report, Technical report, stanford University, 1998.

[Park and Zhao, 2018] Seyoung Park and Hongyu Zhao. Spectral clustering based on learning similarity matrix. *Bioinformatics*, 34(12):2069–2076, 2018.

[Shapiro *et al.*, 2013] Ehud Shapiro, Tamir Biezuner, and Sten Linnarsson. Single-cell sequencing-based technologies will revolutionize whole-organism science. *Nature Reviews Genetics*, 14(9):618–630, 2013.

[Sinkhorn, 1967] Richard Sinkhorn. Diagonal equivalence to matrices with prescribed row and column sums. *The American Mathematical Monthly*, 74(4):402–405, 1967.

[Strehl and Ghosh, 2002] Alexander Strehl and Joydeep Ghosh. Cluster ensembles—a knowledge reuse framework

for combining multiple partitions. *Journal of machine learning research*, 3(Dec):583–617, 2002.

[Tian *et al.*, 2019] Tian Tian, Ji Wan, Qi Song, and Zhi Wei. Clustering single-cell rna-seq data with a model-based deep learning approach. *Nature Machine Intelligence*, 1(4):191–198, 2019.

[Tian *et al.*, 2021] Tian Tian, Jie Zhang, Xiang Lin, Zhi Wei, and Hakon Hakonarson. Model-based deep embedding for constrained clustering analysis of single cell rna-seq data. *Nature communications*, 12(1):1873, 2021.

[Tu *et al.*, 2021] Wenxuan Tu, Sihang Zhou, Xinwang Liu, Xifeng Guo, Zhiping Cai, En Zhu, and Jieren Cheng. Deep fusion clustering network. In *Proceedings of the AAAI Conference on Artificial Intelligence*, volume 35, pages 9978–9987, 2021.

[Van der Maaten and Hinton, 2008] Laurens Van der Maaten and Geoffrey Hinton. Visualizing data using t-sne. *Journal of machine learning research*, 9(11), 2008.

[Van Dijk *et al.*, 2018] David Van Dijk, Roshan Sharma, Juozas Nainys, Kristina Yim, Pooja Kathail, Ambrose J Carr, Cassandra Burdziak, Kevin R Moon, Christine L Chaffer, Diwakar Pattabiraman, et al. Recovering gene interactions from single-cell data using data diffusion. *Cell*, 174(3):716–729, 2018.

[Vinh *et al.*, 2009] Nguyen Xuan Vinh, Julien Epps, and James Bailey. Information theoretic measures for clusterings comparison: is a correction for chance necessary? In *Proceedings of the 26th annual international conference on machine learning*, pages 1073–1080, 2009.

[Wan *et al.*, 2022] Hui Wan, Liang Chen, and Minghua Deng. scname: neighborhood contrastive clustering with ancillary mask estimation for scrna-seq data. *Bioinformatics*, 38(6):1575–1583, 2022.

[Wang *et al.*, 2018] Bo Wang, Daniele Ramazzotti, Luca De Sano, Junjie Zhu, Emma Pierson, and Serafim Batzoglou. Simlr: A tool for large-scale genomic analyses by multi-kernel learning. *Proteomics*, 18(2):1700232, 2018.

[Wang *et al.*, 2021a] Hai-Yun Wang, Jian-ping Zhao, and Chun-Hou Zheng. Suscc: secondary construction of feature space based on umap for rapid and accurate clustering large-scale single cell rna-seq data. *Interdisciplinary Sciences: Computational Life Sciences*, 13:83–90, 2021.

[Wang *et al.*, 2021b] Juexin Wang, Anjun Ma, Yuzhou Chang, Jianting Gong, Yuexu Jiang, Ren Qi, Cankun Wang, Hongjun Fu, Qin Ma, and Dong Xu. scgnn is a novel graph neural network framework for single-cell rna-seq analyses. *Nature communications*, 12(1):1882, 2021.

[Wang *et al.*, 2021c] Zhaokang Wang, Yunpan Wang, Chunfeng Yuan, Rong Gu, and Yihua Huang. Empirical analysis of performance bottlenecks in graph neural network training and inference with gpus. *Neurocomputing*, 446:165–191, 2021.

[Wang *et al.*, 2024] Zaitian Wang, Pengfei Wang, Kunpeng Liu, Pengyang Wang, Yanjie Fu, Chang-Tien Lu, Charu C Aggarwal, Jian Pei, and Yuanchun Zhou. A comprehensive survey on data augmentation. *arXiv preprint arXiv:2405.09591*, 2024.

[Wang *et al.*, 2025] Pengfei Wang, Wenhao Liu, Jiajia Wang, Yana Liu, Pengjiang Li, Ping Xu, Wentao Cui, Ran Zhang, Qingqing Long, Zhilong Hu, et al. sccompass: An integrated multi-species scrna-seq database for ai-ready. *Advanced Science*, page 2500870, 2025.

[Xie *et al.*, 2016] Junyuan Xie, Ross Girshick, and Ali Farhadi. Unsupervised deep embedding for clustering analysis. In *International conference on machine learning*, pages 478–487. PMLR, 2016.

[Xu *et al.*, 2024] Ping Xu, Zhiyuan Ning, Meng Xiao, Guihai Feng, Xin Li, Yuanchun Zhou, and Pengfei Wang. sccdcg: Efficient deep structural clustering for single-cell rna-seq via deep cut-informed graph embedding. In *International Conference on Database Systems for Advanced Applications*, pages 172–187. Springer, 2024.

[Zbontar *et al.*, 2021] Jure Zbontar, Li Jing, Ishan Misra, Yann LeCun, and Stéphane Deny. Barlow twins: Self-supervised learning via redundancy reduction. In *International conference on machine learning*, pages 12310–12320. PMLR, 2021.

[Zhan *et al.*, 2023] Youlin Zhan, Jiahan Liu, and Le Ou-Yang. scmic: a deep multi-level information fusion framework for clustering single-cell multi-omics data. *IEEE Journal of Biomedical and Health Informatics*, 2023.

[Žurauskienė and Yau, 2016] Justina Žurauskienė and Christopher Yau. pcareduce: hierarchical clustering of single cell transcriptional profiles. *BMC bioinformatics*, 17:1–11, 2016.